DR RUTH SOTO (Orcid ID : 0000-0002-1929-8850)

DR ANN HIRT (Orcid ID : 0000-0002-2193-0472)

Article type : Paper

# Triassic stretching directions in Iberia and North Africa inferred from magnetic fabrics

Ruth Soto[1*], Antonio M. Casas-Sainz[2], Belén Oliva-Urcia[3], Cristina García-Lasanta[4], Esther Izquierdo-Llavall[5], Bennacer Moussaid[6], José Carlos Kullberg[7], Teresa Román-Berdiel[2], Yolanda Sánchez-Moya[8], Alfonso Sopeña[8], Sara Torres-López[9], Juan José Villalaín[9], Hamidou El-Ouardi[10], Inmaculara Gil-Peña[11], Ann M. Hirt[12]

[1]Instituto Geológico y Minero de España (IGME). Unidad de Zaragoza, 50006 Zaragoza, Spain

[2]Geotransfer (IUCA). Universidad de Zaragoza. 50009 Zaragoza, Spain

[3]Universidad Autónoma de Madrid, Spain

[4]Western Washington University, Bellingham, WA, United States

[5]Université de Pau et des Pays de l'Adour, France

[6]BGIM Laboratory, ENS Casablanca, Hassan II University, Morocco

[7]Dpto. Ciências da Terra and GeoBioTec, Univ. Nova Lisboa, 2829-516 Caparica, Portugal

[8]Instituto de Geociencias UCM-CSIC, Universidad Complutense de Madrid, Madrid, Spain

[9]Departamento de Física. Universidad de Burgos, Avda. Cantabria, Burgos, Spain

[10]Département de Géologie. Université Moulay Ismail. Meknes, Morocco

[11]Instituto Geológico y Minero de España (IGME). C/Ríos Rosas, Madrid, Spain

[12] Institute of Geophysics. ETH, Zürich, Switzerland

*Corresponding author. Tel.: +34 976 650413; Fax: +34 976 553 358. *E-mail address:* r.soto@igme.es

## Abstract

During the Triassic, Iberia and western North Africa displayed a unique situation in relation with the Central and North Atlantic opening and westward expansion of the Tethys. Unravelling the stretching direction in Triassic deposits of the studied area can help in our understanding of this scenario. The tectonic setting is characterized by localized basins with strong thickness variations greatly influenced by previous post-Variscan mechanical discontinuities. In this work, we revise and compile magnetic fabric data from eight Triassic depocenters in terms of defining the stretching direction (i.e. magnetic lineation), resulting from extensional deformation of this period. Data show the importance of the opening of the Atlantic rift as the leading process during the Triassic. Dextral transtension can explain the deflection of the extensional direction observed in most studied depocenters that is caused by the activity of previous major oblique faults.

**Keywords:** magnetic fabrics, Triassic, Iberia, west North Africa, stretching direction

## Introduction

During the Triassic, the westernmost Tethyan realm records two processes influencing the break-up of Pangea: the initiation of the Central and North Atlantic opening and the westward expansion of the Tethys. The transition between them took place in Iberia and nearby areas of North Africa, controlled by the relative plate motions of the stable cratons of Africa, North America and

Eurasia (e.g. Ziegler, 1990; Redfern et al., 2010; Schettino and Turco, 2011). With respect to the North Atlantic opening, despite the West Iberia-Newfoundland margins have been extensively studied, the first stages of rifting remain poorly understood (e.g. Pérez-Gussinyé, 2013). Based on tectonostratigraphic studies and as other Permo-Triassic basins located along both margins of the Central and North Atlantic (e.g. Withjack and Schlische, 2005; Redfern et al., 2010), the Triassic rifting in Iberia and North Africa is characterized by localized basins with strong thickness variations. They are separated by non-deposition areas, thus indicating an extensional setting strongly conditioned by thermal and mechanical discontinuities in the post-Variscan lithosphere (Sopeña et al., 1988; Arche and López-Gómez, 1996; Van Wees et al., 1998). Towards the East, recent seismic data indicate that the Valencia Trough Basin (east of Iberia) presents a thin continental crust produced by a combination of steep strike-slip faulting and related normal faulting related with the Tethyan rifting (Ranero et al., 2017).

In this work we characterize the extension directions by revising and compiling previous magnetic fabric studies from Iberia and Northern Africa, including Triassic red beds from the Cabuérniga (Western Basque-Cantabrian basin) and Cameros (Demanda massif) basins (Soto et al., 2007, 2008), and Central Pyrenees (Izquierdo-Llavall et al., 2013), which later evolved to an incomplete plate margin between Iberia and Europe (Fig. 1 and Table 1). We also include the Iberian intraplate basins (García-Lasanta et al., 2015), the Lusitanian basin (Soto et al., 2012), and the Western Atlasic Triassic basins (Oliva-Urcia et al., 2016). Further we reinterpret as tectonic magnetic fabrics data related to 21 sites in Triassic sediments from the Southern margin of the Iberian Variscan Massif and the Algarve basin (Dinarés-Turell and Parés, 1996) (Fig. 1 and Table 1). The sedimentological evolution of these basins shows a comparable trend, although not synchronous (e.g. Sopeña et al., 1988). Their opening is linked to continental siliciclastic sedimentation during the Triassic. Maximum thicknesses are reached in the Moroccan Atlantic margin (Eassouira basin), with around 4000 m of continental red beds. In the remainder basins the thickness of these sediments is typically about 1000 m in the depocenters of basins, dramatically thinning towards the faults at their margins. The upper part of these units is characterized by evaporites and red clays: Late Triassic in age in the eastern half of Iberia (Keuper facies), Late Triassic-Early Jurassic in the Western Atlasic basins and Hettangian (Dagorda Formation) in the Lusitanian and Algarve basins. The northeast, east and southern margins of the Iberian Variscan Massif also show shallow marine sediments deposited during Middle-Late Triassic in response to transgressive-regressive cycles related with the westward propagation of the Tethys (e.g. López-Gómez et al., 2002).

In spite of the good outcrop conditions, some of the key features in the extensional history of these Triassic basins remain unknown because of the modification of their original geometry due to the subsequent Late Jurassic-Early Cretaceous rifting and Cenozoic basin inversion. This is the motivation as to why we compile and reinterpret several magnetic fabric studies to characterize the main extensional directions during this particular stage.

## Methodology

Magnetic susceptibility is an anisotropic property that can be expressed geometrically by an ellipsoid with the principal axes Kmax≥Kint≥Kmin (for further explanations e.g. Tarling and Hrouda, 1993; Parés, 2015). Its study is commonly referred to in the literature as anisotropy of magnetic susceptibility (AMS) or magnetic fabric analyses. In extensional settings, the orientation of Kmax (i.e. magnetic lineation) acquired during the early diagenetic stages can indicate the main extension direction during sediment compaction (e.g. Mattei et al., 1997; Soto et al., 2007). All sites revised in this work satisfy the following criteria. (1) They were sampled in weakly deformed deposits, without cleavage and/or penetrative structures to avoid the possible obliteration of the primary extensional magnetic fabric due to the reorientation of phyllosilicates and/or the formation of new mineral phases related to posterior compressional tectonic phases (García-Lasanta et al., 2018 and references therein). (2) All analysed deposits correspond to red beds, a criterion to better compare magnetic fabrics coming from different works, as lithology (i.e. the relative amount of paramagnetic, diamagnetic and ferromagnetic minerals) plays a main role controlling magnetic fabric orientation (e.g. Borradaile and Jackson, 2004). Red beds usually reflect the sum of phyllosilicate and haematite orientations, a magnetic fabric that correlates well with the strain conditions during basinal stage (e.g. Oliva-Urcia et al., 2016 and references therein). (3) Kmin axes of the magnetic susceptibility ellipsoid must be perpendicular to bedding and Kmax axes grouped and within bedding. This feature can help to unravel possible posterior mineralogical artefacts and therefore deletion/alteration of the primary extensional magnetic fabric when it is not satisfied. (4) Comparison with paleocurrent data in equivalent deposits to discard their influence on magnetic fabric orientation and/or check that fine-grained lithologies (claystones and siltstones) indicative of very low-energy environments were sampled.

### Stretching direction inferred from Kmax versus main fault orientation

In the Western Basque-Cantabrian basin in North Iberia, in spite of the small number of sites, a reliable NE-SW lineation can be inferred (Fig. 2). In this area, the main faults are the Cabuérniga and Rumaceo-Golobar faults (García-Espina, 1997), oriented E-W and NW-SE, respectively, whose extensional movements during the Triassic would match well with the deduced stretching direction from magnetic fabric analysis (Fig. 2). The Cabuérniga fault displays a subvertical trace, whereas the Rumaceo-Golobar faults dip north and show a clear positive inversion linked to the Cenozoic compression (García-Espina, 1997). Paleocurrent analysis in Lower Triassic deposits shows a variable trend from N080-070E to N045E upwards (García-Mondéjar et al., 1986).

The southern and northeastern (western Cameros basin) margins of the Iberian Variscan Massif also show a roughly NE-SW extension direction deduced from magnetic fabric analysis (Fig. 2). In western Cameros basin, as in the western Basque-Cantabrian basin, a similar fault network of vertical E-W faults and NW-SE (i.e. South Demanda fault or Pineda de la Sierra fault; Santana-Torre, 2017) faults could explain the deduced stretching direction from Kmax. In the southern margin of the Iberian Variscan Massif, NE-SW to NNE-SSW basement rooted normal faults deforming Neogene sediments (Marín-Lechado et al., 2017) could also be active during the Triassic sedimentation, but their orientation is not coherent with the deduced stretching direction from previous magnetic fabric data in a simple extensional scenario. A more detailed tectonostratigraphic study of the Triassic deposits of this area would be needed to better relate main faults and Kmax orientations.

In the South Branch of the Iberian Chain classically interpreted as an aulacogen (Alvaro et al., 1979), dominant fault directions are NW-SE (e.g. Somolinos fault; Sopeña, 1979) and ENE-WSW (Fig. 2). These two trends result from oblique slip faulting and folding during Cenozoic basin inversion (e.g. De Vicente et al., 2009) but thickness changes in Triassic units allow us to assume that these faults oriented NW-SE and ENE-WSW also controlled Triassic sedimentation. Kmax axes show a main ENE-WSW direction, that has been interpreted as related to a transtensional mechanism of fault movement during the Late Permian-Triassic (García-Lasanta et al., 2015).

In the Central Pyrenees interpretation of AMS results are complicated by the existence of Alpine cleavage and thrust-scale vertical axis rotations in some of the sampled outcrops (Izquierdo-Llaval et al., 2013, 2018) (Table 1). In sites with a sedimentary-type fabric (i.e. without cleavage) and considering magnetic lineation as a passive marker during Alpine deformation, the corrected Kmax coincides with the Pyrenean trend N110ºE and oblique with the preferred N140E stretching direction inferred from syn-sedimentary faults (Izquierdo-Llaval et al., 2013) (Fig. 2). This orientation is consistent with the activity of NNE-SSW-striking normal faults during the deposit of the Lower-

Middle Triassic red-beds that define Stephanian-Triassic Pyrenean basins and reactivated as strike-slip faults during Pyrenean Cenozoic compression (Gisbert, 1981; Izquierdo-Llaval et al., 2013).

Magnetic fabrics in the Lusitanian and Algarve basins show a different pattern. They are not well defined indicating a radial component of extension during basin formation, although a weak preference of WNW-ESE to NW-SE extensional direction is dominant in many sites (Fig. 2). This behavoiur could imply the importance of NE-SW faults (e.g. Arrábida, Arrife, Nazaré and Carcavai faults; Soares et al., 2012; Terrinha et al., 2013) during Triassic sedimentation (Soto et al., 2012).

In Triassic rocks of the Western Atlasic basins magnetic fabrics indicate a well-defined WNW-ESE maximum of Kmax (Oliva-Urcia et al., 2016) (Fig. 2). This orientation is perpendicular to NNE–SSW normal faults dominant in the off- and onshore sectors of the Essaouira basin (e.g. Hafid, 2000) and related with the opening of the Central Atlantic. A secondary maximum oriented NW-SE is also found in sites located eastwards (Asni area). This has been related with a decreasing influence of Atlantic extension towards the continent probably associated with the effect of pre-existing NE-SW faults (e.g. Tizi n'Test fault; Qarbous e tal., 2003), which cross the basement and are parallel to the axis of the Atlasic rift (Oliva-Urcia et al., 2016).

## Geodynamic setting of South Western Europe-Africa Triassic basins and extension directions

All studied areas are located within the frame of extension in the triple junction formed by the Central and North Atlantic and the westernmost Tethys related to the Triassic break-up of Pangea. The Triassic sedimentary units of the analysed basins developed under different conditions that explain their different tectono-sedimentary evolution and variable pattern of stretching directions inferred from magnetic fabrics. The area in which the studied basins are comprised is bounded by three major crustal faults (Manspeizer et al., 1989): the North-Pyrenean fault, the

Cobequid-Chedabucto-Gibraltar fault zone between the future Iberia and Africa, and the South Atlas fault in their southernmost border (Fig. 3). These faults probably showed (at least partially) a strike-slip component (Manspeizer, 1988) thus favoring the development of non-aligned depocenters along the rift axis.

The Lusitanian, Algarve and Western Atlasic basins can be considered as the counterparts of the Triassic basins of North America (Fig. 4; e.g. Withjack et al., 2013), because of the orientation of the main boundary faults; although their character as a continental margin only developed from the Late Triassic onwards. During the Late Triassic the extension directions found in the Lusitanian basin do not agree with a N-S rift (in present-day coordinates) as could be expected from a well defined plate margin as defined by its subsequent basin evolution. This is probably related to (i) the strong influence of inherited faults that cut through the whole lithosphere and conditioned basin geometry more strongly than the extension direction or, alternatively (ii) the influence of thermal doming that would be reflected in the radial extensional regime inferred from AMS in some sites in spite of their relative far position with respect to major CAMP magmatic centers (Hone et al., 2005). Nevertheless, when considering basin evolution in detail, the existence of traverse faults, oblique or completely perpendicular to the N-S rift axis is a non-negligible factor that probably conditioned the local extensional features.

In summary, extension directions obtained in the Lusitanian, Algarve and the Western Atlasic basins can be interpreted to partially reflect strike-slip component that can explain its non-perpendicularity with respect to the rift axis (Fig. 4). According to the obliquity of the extension directions found in the different basins with respect to these major faults, a dextral transtension appears to be the most feasible mechanism during basin formation. The Basque-Cantabrian area and Central Pyrenees show also an extension direction oblique and parallel, respectively, with respect to the North-Pyrenean fault, and consistent with a dextral transtension. In the Pyrenees there is a general agreement on the influence of strike-slip faulting during Stephanian-Permian times that probably extended during the Early Triassic. The Iberian basins may also be affected by strike-slip tectonism during the Triassic. In support of this idea, several works (Sopeña et al., 1988; De Vicente et al., 2009; García-Lasanta et al., 2015) point to a dextral transtension as responsible for the obliquity between master faults which are in turn responsible for subsidence and extension directions. In this case, however, contributing faults show different directions. Through the Triassic, the orientation of the stress regime across Iberia is almost constant, that probably indicates that the opening of the Atlantic rift was the leading process during this time.

Progression of rifting in the Iberian peninsula during the Triassic is also a feature that must be interpreted in the light of the interaction between the Tethys and the Atlantic evolution. Sedimentation and therefore possibly extension was earlier in the northeastern part of Iberia and progressed westwards along the Triassic and Early Jurassic. This progression is also reflected in basin evoution, because similar facies are younger in westwards direction across Iberia (e.g., Sopeña et al., 1988). In any case this diachrony combined with the constant geodynamic pattern point to a long-term extensional to transtensional regime extending during most of Triassic times.

## Conclusion

The stretching direction inferred from magnetic fabrics in the Triassic red beds localized in eight depocenters along Iberia and western North Africa shows a variable pattern with different oriented maxima. This highlights the strong strain compartmentalization of the studied area during the Triassic period. These results are compatible with a regional WNW-ESE stretching direction that is imposed by the Central and North Atlantic opening. The extensional directions obtained in the western portion of Iberia and western Atlasic basins are deviated by the activity of major crustal oblique structures, and that of the eastern half of Iberia are also locally deviated to the NE-SW in relation with the activity of previous oblique structures; these were probably also influenced by the westward spreading of the Tethys. We demonstrate that magnetic lineation is a powerful tool in unraveling the geodynamimc evolution of the opening of the Atlantic rift system.

## Acknowledgements

Funding came from projects CGL2016-77560-C2-1-P and CGL2016-77560-C2-2-P (Spanish Ministry) and the GeoAp Research Group (E01_17R; Aragón Government).

## References

Alvaro, M., Capote, R., Vegas, R., 1979. Un modelo de evolución geotectónica para la Cadena Celtibérica. Acta Geológica Hispánica 14(1), 172-177.

Arche, A., López-Gómez, J., 1996. Origin of the Permian-Triassic Iberian Basin, central eastern Spain. Tectonophysics 266, 443-464.

Borradaile, G.J., Jackson, M., 2004. Anisotropy of magnetic susceptibility (AMS); magnetic petrofabrics of deformed rocks. Geol. Soc. Spec. Publ. 238, 299-360.

De Vicente, G., Vegas, R., Muñoz-Martín, A., Van Wess, J.D., Casas-Sáinz, A., Sopeña, A., Sánchez-Moya, Y., Arche, A., López-Gómez, J., Olaiz, A., Fernández-Lozano, J., 2009. Oblique strain partitioning and transpression on an inverted rift: The Castilian Branch. Tectonophysics 470, 224-242.

Dinarés-Turell, J.D., Parés, J.M., 1996. El Triásico de la Península Ibérica: nuevos datos paleomagnéticos. Cuadernos de Geología Ibérica 20, 367-384.

Fazlikhani, H., Fossen, H., Gawthorpe, R. L., Faleide, J. I., Bell, R. E., 2017. Basement structure and its influence on the structural configuration of the northern North Sea rift. Tectonics 36(6), 1151-1177.

Fisher, R.A., 1953. Dispersion on a sphere. Proc. R. Soc. Lond. A217, 295-305.

García-Espina, R., 1997. La estructura y evolución tectonoestratigráfica del borde occidental de la Cuenca Vasco-Cantábrica en el área de Campóo (Cordillera Cantabrica, NO de España). PhD Thesis, Univ. Oviedo.

García-Lasanta, C., Oliva-Urcia, B., Román-Berdiel, T., Casas, A. M., Gil-Peña, I., Sánchez-Moya, Y., Sopeña, A., Hirt, A.M., Mattei, M., 2015. Evidence for the Permo-Triassic transtensional rifting in the Iberian Range (NE Spain) according to magnetic fabrics results. Tectonophysics 651, 216-231.

García-Lasanta, C., Oliva-Urcia, B., Casas-Sainz, A.M., Román-Berdiel, T., Izquierdo-Llavall, E., Soto, R., Calvín, P., Moussaid, B., El Ouardi, H., Kullberg, J.C., Villalaín, J.J., 2018. Inversion tectonics and magnetic fabrics in Mesozoic basins of the Western Tethys: A review. Tectonophysics 745, 1-23.

García-Mondéjar, J., Pujalte, V., Robles, S., 1986. Características sedimentológicas, secuenciales y tectoestratigráficas del Triásico de Cantabria y norte de Palencia. Cuadernos de Geología Ibérica 10, 151-172.

Gisbert, J., 1981. Estudio geológico-petrológico del Estefaniense-Pérmico de la Sierra del Cadí (Pirineo de Lérida): Diagénesis y Sedimentología (Ph.D. thesis). University of Zaragoza.

Hafid, M., 2000. Triassic-early Jurassic extensional systems and their Tertiary inversion, Essaouira basin (Morocco). Marine and Petroleum Geology 17, 409-429.

Hone, J.G., Anderson, D.L., Beutel, E.K., Fialko, Y.A., 2005. Giant dikes, rifts, flood basalts, and plate tectonics: A contention of mantle models. In: Foulger, G.R., Natland, J.H., Pressnall, D.C. and Anderson, D.L. (eds.) Plates, plumes and paradigms. Geological Society of America Special Paper 388, 401-420.

Izquierdo-Llavall, E., Casas-Sainz, A. M., Oliva-Urcia, B., 2013. Heterogeneous deformation recorded by magnetic fabrics in the Pyrenean Axial Zone. Journal of Structural Geology 57, 97-113.

Izquierdo- Llavall, E., Casas- Sainz, A. M., Oliva- Urcia, B., Villalaín, J. J., Pueyo, E., Scholger, R., 2018. Rotational kinematics of basement antiformal stacks: paleomagnetic study of the western Nogueras Zone (Central Pyrenees). Tectonics 37(10), 3456-3478.

Jelinek, V., 1981. Characterization of the magnetic fabrics of rocks. Tectonophysics 79, 63-67.

Le Roy, P., Piqué, A., 2001. Triassic–Liassic Western Moroccan synrift basins in relation to the Central Atlantic opening. Marine Geology 172(3-4), 359-381.

López-Gómez, J., Arche, A., Pérez-López, A., 2002. Permian and Triassic. In: Gibbons, W., Moreno, M.T. (Eds.), The Geology of Spain, Geol. Soc., London, pp. 185– 212.

Marín- Lechado, C., Pedrera, A., Peláez, J. A., Ruiz- Constán, A., González- Ramón, A., Henares, J., 2017. Deformation style and controlling geodynamic processes at the eastern Guadalquivir foreland basin (Southern Spain). Tectonics 36(6), 1072-1089.

Manspeizer, W., 1988. Triassic-Jurassic rifting and opening of the Atlantic: an overview. In Developments in Geotectonics Vol. 22, pp. 41-79. Elsevier.

Manspeizer, W., DeBoer, J., Costain, J. K., Froelich, A. J., Coruh, C., Olsen, P. E., McHone, G.J., Puffer, J.H., Thomas, W. A., 1989. Post-Paleozoic activity. The Appalachian-Ouachita orogen in the

United States: Boulder, Colorado, Geological Society of America, Geology of North America, 319-374.

Mattei, M., Sagnotti, L., Faccenna, C., Funiciello, R., 1997. Magnetic fabric of weakly deformed clay-rich sediments in the Italian peninsula: Relationship with compressional and extensional tectonics. Tectonophysics 271, 107–122.

Mosar, J., Eide, E. A., Osmundsen, P. T., Sommaruga, A., Torsvik, T. H., 2002. Greenland–Norway separation: a geodynamic model for the North Atlantic. Norwegian Journal of Geology 82, 282.

Oliva-Urcia, B., Casas, A. M., Moussaid, B., Villalaín, J. J., El Ouardi, H., Soto, R., Torres-López, S., Román-Berdiel, T., 2016. Tectonic fabrics vs. mineralogical artifacts in AMS analysis: A case study of the Western Morocco extensional Triassic basins. Journal of Geodynamics 94, 13-33.

Olsen, P. E. 1997. Stratigraphic record of the early Mesozoic breakup of Pangea in the Laurasia-Gondwana rift system. Annual Reviews of Earth and Planetary Science 25, 337-401.

Parés, J.M., 2015. Sixty years of anisotropy of magnetic susceptibility in deformed sedimentary rocks. Frontiers in Earth Science 3, 4.

Pérez-Gussinyé, M., 2013. A tectonic model for hyperextension at magma-poor rifted margins: an example from the West Iberia–Newfoundland conjugate margins. Geological Society, London, Special Publications 369(1), 403-427.

Qarbous, A., Medina, F., Hoepffner, C., 2003. Le bassin de Tizi n'Test (Haut Atlas, Maroc): Exemple d'évolution d'un segment oblique au rift de l'Atlantique central au Trias. Can. J. Earth Sci. 40, 949-964.

Ranero, C.R., Cameselle, L.A., Viñas, M., 2017. Tethys Rifting in the Valencia Trough basin. In AGU Fall Meeting Abstracts.

Redfern, J., Shannon, P. M., Williams, B. P. J., Tyrrell, S., Leleu, S., Perez, I. F., Baudon, C. Stolfová, K., Hodgetts, D., Van Lanen, X., Speksnijder, A., Haughton, P.D.W., Daly, J.S., 2010. An integrated study of Permo-Triassic basins along the North Atlantic passive margin: implication for future exploration. In Geological Society, London, Petroleum Geology Conference series (Vol. 7, No. 1, pp. 921-936). Geological Society of London.

Roberts, D. G., Thompson, M., Mitchener, B., Hossack, J., Carmichael, S., Bjornseth, H.M. 1999. Palaeozoic to Tertiary Rift and Basin Dynamics: mid-Norway to the Bay of Biscay - a new context for hydrocarbon prospectivity in the deep water frontier. In: Fleet, A. J., Boldy, S. A. R. (eds) Petroleum Geology of Northwest Europe: Proceedings of the 5th Conference, 7-40. Petroleum Geology '86 Ltd. Published by the Geological Society, London.

Santana-Torre, V. J. S., 2017. Estructura del paleozoico del borde sur-occidental de la Sierra de la Demanda. Revista de la Sociedad Geológica de España, 30(2), 27-36.

Schettino, A., Turco, E., 2011. Tectonic history of the western Tethys since the Late Triassic. GSA Bulletin 123(1-2), 89-105.

Soares, A. F., Kullberg, J. C., Marques, J. F., da Rocha, R. B., Callapez, P. M., 2012. Tectono-sedimentary model for the evolution of the Silves Group (Triassic, Lusitanian basin, Portugal). Bulletin de la Société géologique de France 183(3), 203-216.

Sopeña, A., 1979. Estratigrafía del Pérmico y Triásico del Noroeste de la Provincia de Guadalajara. Seminarios de Estratigrafía Serie Monografías 5. Editorial de la Universidad Complutense, Madrid (329 pp.).

Sopeña, A., López, J., Arche, A., Pérez-Arlucea, M., Ramos, A., Virgili, C., Hernando, S., 1988. Permian and Triassic rift basins of the Iberian Peninsula. In: Manspeizer, W. (Ed.), Triassic-Jurassic Rifting. Developments in Geotectonics, 22-B. Elsevier, Amsterdam, pp. 757-786.

Soto, R., Casas-Sainz, A.M., Villalaín, J.J., Oliva-Urcia, B., 2007. Mesozoic extension in the Basque-Cantabrian basin (N Spain. Contributions from AMS and brittle mesostructures. Tectonophysics 445, 373–394.

Soto, R., Casas-Sainz, A.M., Villalaín, J.J., Gil-Imaz, A., Fernández-González, G., Del Río, P., Calvo, M., Mochales, T., 2008. Characterizing the Mesozoic extension direction in the northern Iberian plate margin by anisotropy of magnetic susceptibility (AMS). J. Geol. Soc. Lond. 165, 1007–1018.

Soto, R., Kullberg, J.C., Oliva-Urcia, B., Casas-Sainz, A.M., Villalaín, J.J., 2012. Switch of Mesozoic extensional tectonics style in the Lusitanian basin (Portugal). Insights from magnetic fabrics. Tectonophysics 536–537, 122–135.

Tarling, D.H., Hrouda, F., 1993. The magnetic anisotropy of rocks. Champman & Hall (215 pp.).

Van Wees, J.D., Arche, A., Beijdorff, C.G., Lopez-Gomez, J., Cloetingh, S., 1998. Temporal and spatial variations in tectonic subsidence in the Iberian Basin (E Spain). Tectonophysics 300, 285–310.

Terrinha, P., Rocha, R.B., Rey, J., Cachão, M., Moura, D., Roque, C., Martins, L., Valadares, V., Cabral, J., Azevedo, M.R., Barbero, L., González Clavijo, E.J., Dias, R.P., Matias, H., Madeira, C.M., Silva, Munhã, J., Rebêlo, L.P., Ribeiro, C., Vicente, J., Noiva, J., Youbi, N., Bensalah, M.K., 2013. A Bacia do Algarve: Estratigrafia, Paleogeografia e Tectónica. In: R. Dias, A. Araújo, P. Terrinha. J.C. Kullberg, (Eds). Geologia de Portugal, Vol. II, Geologia Meso-cenozóica de Portugal. Escolar Editora. II: 29-166.

Withjack, M. O., Schlische, R. W., 2005. A review of tectonic events on the passive margin of eastern North America. In Petroleum Systems of Divergent Continental Margin Basins: 25th Bob S. Perkins Research Conference, Gulf Coast Section of SEPM (pp. 203-235). SEPM.

Withjack, M. O., Schlische, R. W., Malinconico, M. L., Olsen, P. E., 2013. Rift-basin development: lessons from the Triassic–Jurassic Newark Basin of eastern North America. Geological Society, London, Special Publications 369(1), 301-321.

Ziegler, P.A., 1990. Geological Atlas of Western and Central Europe, Shell Internationale Petroleum Maatschappij BV/Geological Society of London, 239 pp.

## Figure captions

-Figure 1. Location of studied areas with Triassic outcrops and suitable magnetic fabric data (see text for details).

-Figure 2. Stereoplots showing Kmax (average value for site) after tectonic correction and their density plot (C.I.=2.0%/1% area) (except for 1 and 2 which do not have statistical meaning as they comprise only 4 specimens) and rose diagram. Map showing main faults active during the Triassic in the studied areas (see text for details). N indicates the number of sites (average value showed in Table 1) and n indicates number of specimens extracted from stereoplots in Dinarés-Turell and Parés (1996). Lower-hemisphere equal-area stereoplots.

-Figure 3. A. Reconstruction of Pangea for Carnian (modified from Olsen, 1997). B. Simplified tectonic map of the main Variscan tectonic elements of Europe, Africa and North America and Triassic rifting (modified from Manspeizer et al., 1989) showing the stretching directions inferred from magnetic fabrics in Iberia and North Africa.

-Figure 4. A. Geodynamic setting of the Triassic sedimentary basins of Europe, western North Africa and North America showing the main faults influencing basin distribution and sedimentation and stretching directions inferred from magnetic fabrics. Paleogeographic reconstruction for the Triassic prior to oceanic spreading modified from Ziegler (1990) and Le Roy and Piqué (2001). Triassic normal faults of eastern North America (from Withjack et al., 2013), western North Africa (from Hafid, 2000), North Sea (from Roberts et al., 1999) and Norwegian Sea (from Fazlikhani et al., 2017) are also drawn together with the Triassic extensional directions from Withjack and Schlische (2005) and Mosar et al. (2002). B. Interpretation in terms of rifting and transform major faults in present-day coordinates.

## Table captions

**-Table 1.** Magnetic fabric data (as listed in the reviewed contributions).

| # | Site | Lithology | Age | n | D/I(Kmax) In situ | E11.1 ($e_{12}$/$e_{13}$) | D/I(Kmin) In situ | E11.3 ($e_{13}$/$e_{23}$) or $\alpha_{95}$ | D/I(Kmax) Corrected | Km ($10^{-6}$) | P’ | T | Bedding pole |
|---|---|---|---|---|---|---|---|---|---|---|---|---|---|
| ***Lusitanian basin (from Soto et al., 2012)*** | | | | | | | | | | | | | |
| 1 | LU01 | Fine sandstone | Late Triassic | 22 | 193/6 | 13.0/4.9 | 073/79 | 16.6/5.1 | 194/4 | 122 | 1.047 | 0.668 | 093,80 |
| 2 | LU02 | Red sandstone | Late Triassic | 5 | 292/10 | 13.9/4.2 | 096/79 | 18.5/5.8 | 112/5 | 147 | 1.021 | 0.678 | 115,75 |
| 3 | LU03 | Red sandstone | Late Triassic | 20 | 211/10 | 38.6/6.3 | 070/77 | 7.2/3.7 | 213/0 | 150 | 1.052 | 0.854 | 090,72 |
| 4 | LU04 | Red clay | Hettangian | 9 | 139/22 | 39.5/12.1 | 277/61 | 13.9/9.6 | 138/15 | 294 | 1.083 | 0.822 | 290,82 |
| 5 | LU05 | Red sandstone | Late Triassic | 16 | 063/4 | 56.2/8.6 | 196/84 | 22.9/7.2 | 063/3 | 110 | 1.033 | 0.268 | bed. subhor. |
| 6 | LU06 | Red fine lutite | Hettangian | 10 | 273/3 | 35.6/5.5 | 157/84 | 7.4/5.3 | 093/2 | 329 | 1.076 | 0.885 | 050,84 |
| 7 | LU07 | Red sandstone | Late Triassic | 12 | 299/5 | 17.7/6.5 | 050/75 | 7.5/6.5 | 119/8 | 87.0 | 1.020 | 0.732 | 107,76 |
| 8 | LU08 | Sandstone | Late Triassic | 10 | 113/11 | 63.1/14.3 | 255/77 | 20.7/11.8 | 292/14 | 137 | 1.022 | 0.599 | 305,65 |
| 9 | LU09 | Red lutite | Late Triassic | 13 | 058/9 | 43.2/6.2 | 285/76 | 11.1/4.5 | 059/7 | 182 | 1.020 | 0.782 | 316,80 |
| 10 | LU10 | Red sandstone | Late Triassic | 12 | 110/9 | 14.3/4.1 | 248/78 | 7.7/4.5 | 111/10 | 153 | 1.034 | 0.847 | 040,85 |
| 11 | LU11 | Sandstone/Lutite | Late Triassic | 28 | 273/9 | 71.6/7.8 | 053/78 | 10.7/7.2 | 273/9 | 97.3 | 1.033 | 0.614 | bed. subhor. |
| 12 | LU12 | Red clay | Hettangian | 12 | 360/5 | 20.9/7.8 | 175/85 | 11.6/6.7 | 360/3 | 239 | 1.090 | 0.842 | 095,78 |
| 13 | LU13 | Red sandstone | Hettangian | 22 | 219/11 | 25.7/4.3 | 334/66 | 7.0/4.2 | 038/5 | 208 | 1.082 | 0.864 | 346,64 |
| 14 | LU14 | Red fine sandstone | Late Triassic | 24 | 109/25 | 21.4/4.2 | 247/58 | 7.1/4.0 | 108/6 | 211 | 1.036 | 0.763 | 285,71 |
| 15 | LU15 | Red sandstone | Late Triassic | 12 | 303/13 | 38.2/22.5 | 141/76 | 23.5/18.2 | 301/0 | 171 | 1.053 | 0.587 | 071,69 |
| 16 | LU16 | Red fine sandstone | Late Triassic | 9 | 179/5 | 11.0/3.6 | 037/83 | 16.9/3.7 | 180/1 | 138 | 1.030 | 0.531 | 076,73 |
| 17 | LU17 | Red clay | Late Triassic | 11 | 157/0 | 31.4/7.7 | 254/86 | 11.8/5.6 | 157/2 | 135 | 1.035 | 0.792 | 198,88 |
| 18 | LU18 | Red clay | Late Triassic | 11 | 229/7 | 39.1/5.0 | 109/77 | 8.5/5.1 | 049/6 | 307 | 1.074 | 0.829 | 082,75 |
| 19 | LU19 | Orange clay | Hettangian | 16 | 299/7 | 36.0/9.6 | 096/82 | 10.1/9.4 | 119/24 | 158 | 1.079 | 0.873 | 113,58 |
| ***Cabuérniga basin (from Soto et al., 2007)*** | | | | | | | | | | | | | |
| 20 | CAT1 | Red bed | Early Triassic | 8 | 004/32 | 19.0/4.0 | 174/58 | 6.0º ($\alpha_{95}$) | 002/1 | 102.01 | 1.038 | 0.2 | 170, 58 |
| 21 | CAT2 | Red bed | Early Triassic | 18 | 036/25 | 10.1/3.8 | 212/65 | 3.3º ($\alpha_{95}$) | 035/1 | 163.3 | 1.05 | 0.613 | 214, 66 |
| 22 | CAT3 | Red bed | Early Triassic | 16 | 281/62 | 12.2/6.9 | 175/36 | 5.7º ($\alpha_{95}$) | 206/5 | 82.76 | 1.069 | 0.642 | 358, 0 |
| 23 | CAT4 | Red bed | Early Triassic | 23 | 053/28 | 6.5/5.7 | 202/57 | 3.9º ($\alpha_{95}$) | 232/1 | 145 | 1.028 | 0.455 | 218, 60 |
| ***Demanda-Cameros massif (from Soto et al., 2008)*** | | | | | | | | | | | | | |
| 24 | TPO1 | Red bed | Early Triassic | 15 | 107/59 | 59.0/14.6 | 002/47 | - | 034/14 | 119.5 | 1.017 | 0.548 | 183, 8 |
| 25 | TPO10 | Red bed | Early Triassic | 23 | 229/1 | 18.3/8.9 | 305/76 | 14.2º ($\alpha_{95}$) | 050/7 | 95.4 | 1.017 | 0.150 | 340, 67 |
| 26 | TVI3 | Red bed | Early Triassic | 21 | 075/4 | 34.1/17.3 | 153/55 | - | 253/1 | 103.9 | 1.023 | 0.510 | 169, 38 |
| 27 | TVI1 | Red bed | Middle-Late Triassic | 27 | 215/9 | 34.0/18.9 | 99/70 | 13.7º ($\alpha_{95}$) | 034/5 | 126.6 | 1.031 | 0.520 | 344, 68 |
| ***Central Pyrenean basins (from Izquierdo-Llavall et al., 2013)*** | | | | | | | | | | | | | |
| 28 | TP1 (*-4º) | Sandstone | Early-Middle Triassic | 12 | 286/17 | 8/4 | 033/43 | 6/3 | 105/6 * | 55 | 1.040 | 0.505 | 37,35 |
| 29 | TP3 (*+19º) | Sandstone /Shales | Early-Middle Triassic | 16 | 106/35 | 20/13 | 197/01 | 18/8 | 121/2 * | 136 | 1.033 | 0.326 | 15,5 |
| 30 | TP5 (*0º) | Sandstone | Early-Middle Triassic | 14 | 130/05 | 13/3 | 039/07 | 11/3 | 304/13 | 147 | 1.057 | 0.380 | 24,18 |
| 31 | TP8 (*0º) | Shales/Sandstone | Early-Middle Triassic | 13 | 305/05 | 6/4 | 040/46 | 8/4 | 116/10 | 127 | 1.038 | -0.343 | 30,39o |
| 32 | TP9 (*+34º) | Shales | Early-Middle Triassic | 15 | 121/03 | 13/7 | 213/33 | 10/10 | 266/3 * | 189 | 1.047 | 0.192 | 200,45o |
| 33 | TP11 (*+18º) | Sandstone | Early-Middle Triassic | 31 | 105/20 | 14/7 | 013/06 | 11/7 | 111/6 * | 162 | 1.081 | 0.725 | 20,2o |
| 34 | TP14 (*+38º) | Sandstone | Early-Middle Triassic | 22 | 299/13 | 32/09 | 050/56 | 10/7 | 072/6 * | 78 | 1.044 | 0.67 | 40,54o |
| 35 | TP15 (*+13º) | Shales | Early-Middle Triassic | 19 | 304/11 | 14/10 | 198/56 | 15/4 | 103/8 * | 221 | 1.081 | 0.255 | 214,48o |
| 36 | TP16 (*+39º) | Sandstone | Early-Middle Triassic | 16 | 136/08 | 13/5 | 235/50 | 8/5 | 281/6 * | 128 | 1.069 | 0.782 | 225,43o |
| 37 | TP22 (*+38º) | Shales/Sandstone | Early-Middle Triassic | 19 | 083/16 | 26/5 | 183/31 | 6/5 | 093/6 * | 149 | 1.119 | 0.775 | 195,40o |
| 38 | TP23 (*+36º) | Sandstone | Early-Middle Triassic | 19 | 050/12 | 19/5 | 164/61 | 9/4 | 104/3 * | 158 | 1.164 | 0.887 | 159,60o |

| | | | | | | | | | | | | | |
|---|---|---|---|---|---|---|---|---|---|---|---|---|---|
| 39 | TP27 (*+43º) | Sandstone | Early-Middle Triassic | 25 | 256/07 | 26/4 | 164/20 | 10/4 | 045/11 * | 113 | 1.077 | 0.87 | 180,15o |
| 40 | TP28 (*+38º) | Sandstone | Early-Middle Triassic | 8 | 026/67 | 18/9 | 223/22 | 9/5 | 248/47 * | 35 | 1.048 | 0.484 | 150,38 |
| 41 | TP29 (*+58º) | Shales/Sandstone | Early-Middle Triassic | 20 | 101/39 | 24/8 | 241/44 | 11/11 | 151/8 * | 209 | 1.08 | 0.755 | 240,35o |
| 42 | TP34 (*+67º) | Sandstone | Early-Middle Triassic | 21 | 153/34 | 54/09 | 055/11 | 9/4 | 039/2 * | 136 | 1.061 | 0.826 | 52,13o |
| 43 | TP35 (*+9º) | Shales | Early-Middle Triassic | 26 | 108/04 | 9/7 | 201/29 | 10/7 | 111/3 * | 197 | 1.045 | 0.428 | 204,28o |
| 44 | TP39 (*+20º) | Shales/Sandstone | Early-Middle Triassic | 25 | 123/03 | 9/4 | 032/30 | 13/8 | 107/3 * | 174 | 1.041 | 0.102 | 35,26 |
| 45 | TP40 (*+47º) | Shales | Early-Middle Triassic | 24 | 270/22 | 11/8 | 138/59 | 12/5 | 227/11 * | 84 | 1.024 | 0.024 | 138,74 |
| ***Iberian basin (from García-Lasanta et al., 2015)*** | | | | | | | | | | | | | |
| 46 | RE1 | Red bed | Permian-Early Triassic | 11 | 011/4 | 19/10 | 113/72 | 17/13 | 191/9 | 189 | 1.031 | 0.328 | 170,76 |
| 47 | RE2 | Red bed | Permian-Early Triassic | 15 | 245/1 | 24/6 | 137/87 | 6/4 | 245/8 | 140 | 1.020 | 0.745 | 192,79 |
| 48 | RE3 | Red bed | Permian-Early Triassic | 13 | 358/6 | 22/6 | 252/71 | 20/6 | 358/6 | 139 | 1.031 | 0.652 | 270,90 |
| 49 | RE4 | Red bed | Late Triassic | 9 | 287/6 | 11/5 | 053/80 | 16/4 | 288/44 | 147 | 1.038 | 0.786 | 179,85 |
| 50 | RE5 | Red bed | Middle Triassic | 23 | 270/8 | 10/6 | 160/67 | 8/3 | 273/8 | 271 | 1.072 | 0.701 | 179,68 |
| 51 | RE6 | Red bed | Late Triassic | 25 | 310/9 | 31/6 | 189/74 | 7/4 | 130/1 | 191 | 1.137 | 0.821 | 179,75 |
| 52 | RE7 | Red bed | Permian-Early Triassic | 15 | 321/8 | 52/5 | 188/79 | 16/3 | 322/8 | 215 | 1.022 | 0.760 | 270,90 |
| 53 | RE8 | Red bed | Permian-Early Triassic | 19 | 301/5 | 34/8 | 199/68 | 9/4 | 121/6 | 217 | 1.052 | 0.850 | 179,70 |
| 54 | RE9 | Red bed | Late Triassic | 14 | 320/9 | 69/4 | 179/78 | 10/4 | 140/11 | 122 | 1.032 | 0.888 | 175,65 |
| 55 | RE10 | Red bed | Permian-Early Triassic | 12 | 056/5 | 21/14 | 310/73 | 45/13 | 236/10 | 105 | 1.047 | 0.686 | 191,69 |
| 56 | RE11 | Red bed | Permian-Early Triassic | 17 | 255/4 | 14/3 | 048/86 | 10/3 | 075/2 | 200 | 1.031 | 0.874 | 30,82 |
| 57 | RE12 | Red bed | Permian-Early Triassic | 18 | 260/1 | 29/10 | 354/72 | 11/4 | 260/1 | 193 | 1.029 | 0.844 | 350,73 |
| 58 | RE13 | Red bed | Permian-Early Triassic | 12 | 022/2 | 26/8 | 190/88 | 10/4 | 022/10 | 221 | 1.028 | 0.602 | 20,82 |
| 59 | CO1 | Red bed | Permian-Early Triassic | 8 | 003/3 | 49/5 | 147/87 | 7/5 | 003/3 | 250 | 1.059 | 0.890 | 270,90 |
| 60 | CO2 | Red bed | Permian-Early Triassic | 12 | 033/4 | 81/3 | 166/84 | 5/4 | 031/7 | 296 | 1.083 | 0.919 | 96,83 |
| 61 | CO3 | Red bed | Permian-Early Triassic | 34 | 305/7 | 68/5 | 105/82 | 13/5 | 306/6 | 167 | 1.042 | 0.854 | 179,88 |
| 62 | AL1 | Red bed | Permian-Early Triassic | 9 | 255/12 | 21/8 | 058/78 | 12/4 | 256/3 | 198 | 1.049 | 0.551 | 77,81 |
| 63 | AL2 | Red bed | Permian-Early Triassic | 15 | 344/11 | 24/9 | 114/73 | 16/10 | 345/6 | 98.3 | 1.014 | 0.446 | 179,85 |
| 64 | AL3 | Red bed | Permian-Early Triassic | 16 | 090/41 | 35/9 | 321/36 | 14/10 | 110/4 | 194 | 1.064 | 0.895 | 331,34 |
| 65 | AL4 | Red bed | Permian-Early Triassic | 13 | 078/14 | 31/12 | 255/73 | 13/8 | 078/2 | 202 | 1.046 | 0.650 | 275,77 |
| 66 | AL5 | Red bed | Late Triassic | 12 | 303/15 | 30/6 | 168/69 | 16/5 | 304/14 | 221 | 1.057 | 0.878 | 179,88 |
| 67 | AL6 | Red bed | Permian-Early Triassic | 12 | 215/2 | 21/9 | 355/87 | 13/5 | 216/7 | 159 | 1.087 | 0.760 | 187,84 |
| 68 | AL7 | Red bed | Middle Triassic | 9 | 298/5 | 29/11 | 192/71 | 12/11 | 299/6 | 204 | 1.079 | 0.781 | 213,80 |
| 69 | AL8 | Red bed | Permian-Early Triassic | 13 | 274/8 | 44/9 | 139/78 | 11/11 | 094/2 | 188 | 1.029 | 0.653 | 100,80 |
| 70 | AL9 | Red bed | Permian-Early Triassic | 12 | 81/13 | 21/6 | 237/76 | 11/6 | 081/12 | 237 | 1.059 | 0.519 | 179,88 |
| 71 | RS1 | Red bed | Permian-Early Triassic | 16 | 073/44 | 37/11 | 313/27 | 14/8 | 096/8 | 165 | 1.037 | 0.640 | 316,35 |
| 72 | RS2 | Red bed | Permian-Early Triassic | 10 | 234/2 | 24/6 | 325/25 | 7/3 | 229/8 | 204 | 1.058 | 0.740 | 316,35 |
| 73 | RS3 | Red bed | Permian-Early Triassic | 16 | 207/12 | 55/11 | 308/44 | 13/5 | 022/2 | 209 | 1.067 | 0.798 | 308,35 |
| 74 | RS4 | Red bed | Permian-Early Triassic | 14 | 256/7 | 17/6 | 140/74 | 6/5 | 076/2 | 163 | 1.060 | 0.725 | 120,78 |
| 75 | RS5 | Red bed | Permian-Early Triassic | 21 | 280/3 | 39/6 | 172/80 | 14/6 | 100/14 | 144 | 1.059 | 0.860 | 115,72 |
| 76 | RS6 | Red bed | Middle Triassic | 14 | 245/0 | 27/4 | 338/87 | 9/4 | 065/1 | 229 | 1.045 | 0.899 | 150,80 |
| 77 | RS7 | Red bed | Permian-Early Triassic | 14 | 254/14 | 12/4 | 104/74 | 22/5 | 075/8 | 128 | 1.061 | 0.884 | 107,64 |
| 78 | RS8 | Red bed | Middle Triassic | 12 | 076/0 | 18/6 | 167/79 | 11/7 | 075/5 | 190 | 1.063 | 0.623 | 140,80 |
| 79 | RS9 | Red bed | Permian-Early Triassic | 13 | 268/9 | 59/11 | 139/77 | 12/9 | 269/14 | 109 | 1.015 | 0.550 | 210,80 |
| 80 | RS10 | Red bed | Permian-Early Triassic | 17 | 066/28 | 45/10 | 286/55 | 13/5 | 252/1 | 244 | 1.028 | 0.569 | 290,52 |
| 81 | RS11 | Red bed | Late Triassic | 16 | 102/46 | 37/8 | 352/18 | 8/6 | 310/4 | 190 | 1.053 | 0.743 | 350,15 |
| 82 | RS12 | Red bed | Late Triassic | 7 | 053/16 | 26/10 | 246/74 | 28/10 | 053/16 | 186 | 1.037 | 0.440 | 270,90 |

| | | | | | | | | | | | | | |
|---|---|---|---|---|---|---|---|---|---|---|---|---|---|
| 83 | SI1 | Red bed | Permian-Early Triassic | 9 | 090/2 | 19/3 | 191/80 | 14/2 | 089/5 | 172 | 1.064 | 0.949 | 165,79 |
| 84 | SI2 | Red bed | Permian-Early Triassic | 9 | 289/2 | 28/9 | 085/88 | 9/4 | 289/2 | 162 | 1.060 | 0.896 | 270,90 |
| 85 | SI3 | Red bed | Permian-Early Triassic | 10 | 249/6 | 16/3 | 358/72 | 4/3 | 248/1 | 191 | 1.057 | 0.703 | 353,74 |
| 86 | SI4 | Red bed | Permian-Early Triassic | 12 | 256/3 | 32/14 | 153/75 | 15/10 | 076/3 | 145 | 1.036 | 0.780 | 86,84 |
| 87 | SI5 | Red bed | Permian-Early Triassic | 15 | 337/7 | 25/7 | 138/83 | 9/6 | 156/5 | 116 | 1.038 | 0.630 | 129,77 |
| 88 | SI6 | Red bed | Middle Triassic | 24 | 148/27 | 25/3 | 358/59 | 3/2 | 332/1 | 76.6 | 1.037 | 0.814 | 0,58 |
| 89 | SI7 | Red bed | Middle Triassic | 33 | 062/9 | 16/4 | 313/63 | 7/5 | 245/2 | 52.1 | 1.041 | 0.200 | 318,50 |
| 90 | RO1 | Red bed | Permian-Early Triassic | 10 | 307/2 | 8/4 | 041/64 | 16/4 | 127/1 | 203 | 1.033 | 0.090 | 175,85 |
| 91 | RO2 | Red bed | Permian-Early Triassic | 24 | 068/4 | 24/4 | 167/64 | 4/3 | 065/9 | 211 | 1.058 | 0.844 | 145,65 |
| 92 | RO3 | Red bed | Permian-Early Triassic | 9 | 089/7 | 16/4 | 193/63 | 15/5 | 089/7 | 121 | 1.046 | 0.616 | 270,90 |
| 93 | RO4 | Red bed | Permian-Early Triassic | 21 | 256/12 | 8/2 | 141/64 | 3/2 | 262/16 | 84.4 | 1.028 | 0.613 | 179,65 |
| 94 | YE1 | Red bed | Permian-Early Triassic | 8 | 071/4 | 27/5 | 205/85 | 6/4 | 250/4 | 132 | 1.037 | 0.778 | 245,82 |
| 95 | YE2 | Red bed | Late Triassic | 13 | 255/11 | 24/10 | 000/54 | 11/5 | 072/6 | 195 | 1.055 | 0.837 | 0,35 |
| 96 | AJ1 | Red bed | Permian-Early Triassic | 14 | 129/4 | 37/4 | 293/86 | 11/3 | 129/7 | 194 | 1.053 | 0.916 | 86,85 |
| 97 | AJ2 | Red bed | Permian-Early Triassic | 14 | 310/1 | 28/5 | 217/72 | 13/6 | 313/7 | 142 | 1.053 | 0.868 | 230,50 |
| 98 | AJ3 | Red bed | Permian-Early Triassic | 17 | 116/1 | 17/4 | 214/84 | 5/4 | 116/1 | 210 | 1.064 | 0.844 | 270,90 |
| 99 | AJ4 | Red bed | Permian-Early Triassic | 13 | 093/3 | 36/6 | 232/86 | 8/4 | 093/3 | 259 | 1.075 | 0.903 | 270,90 |
| 100 | AJ5 | Red bed | Middle Triassic | 17 | 358/16 | 30/6 | 236/62 | 8/5 | 181/4 | 177 | 1.054 | 0.884 | 228,60 |
| ***West Atlasic basins (from Oliva-Urcia et al., 2016)*** | | | | | | | | | | | | | |
| 101 | AG2 | Red bed | Triassic | 15 | 306/9 | 20/11 | 211/25 | 18/5 | 321/14 | 115 | 1.055 | 0.651 | 227,35 |
| 102 | AG3 | Red bed | Triassic | 23 | 062/42 | 71/35 | 209/43 | 35/28 | 052/12 | 68.7 | 1.009 | -0.046 | 204,55 |
| 103 | AG4 | Red bed | Triassic | 12 | 057/32 | 22/8 | 205/53 | 10/9 | 051/0 | 89.8 | 1.042 | 0.456 | 207,53 |
| 104 | AG8 | Red bed | Triassic | 15 | 290/57 | 59/26 | 091/31 | 30/24 | 283/21 | 104 | 1.015 | 0.104 | 115,52 |
| 105 | AG11 | Red bed | Triassic | 20 | 089/1 | 28/6 | 357/53 | 11/5 | 087/4 | 60.1 | 1.019 | 0.426 | 004,48 |
| 106 | AG12 | Red bed | Triassic | 9 | 071/20 | 14/3 | 181/43 | 11/3 | 064/3 | 368 | 1.025 | 0.202 | 185,54 |
| 107 | AG16 | Red bed | Triassic | 18 | 273/3 | 27/4 | 061/87 | 7/4 | 093/3 | 107 | 1.023 | 0.385 | 070,84 |
| 108 | AG17 | Red bed | Triassic | 17 | 274/6 | 17/15 | 167/71 | 19/15 | 279/9 | 103 | 1.025 | 0.518 | 191,51 |
| 109 | AG20 | Red bed | Triassic | 14 | 089/16 | 26/11 | 209/60 | 11/5 | 084/6 | 82.7 | 1.036 | 0.473 | 206,70 |
| 110 | AG21 | Red bed | Triassic | 11 | 267/15 | 24/20 | 144/63 | 25/20 | 090/3 | 41.9 | 1.028 | 0.016 | 146,57 |
| 111 | AG22 | Red bed | Triassic | 5 | 283/67 | 14/4 | 083/21 | 10/1 | 095/3 | 92.5 | 1.051 | 0.326 | 090,19 |
| 112 | AG28 | Red bed | Triassic | 23 | 287/5 | 26/16 | 183/70 | 40/17 | 105/12 | 49.6 | 1.018 | -0.024 | 174,42 |
| 113 | AG29 | Red bed | Triassic | 20 | 297/5 | 32/20 | 070/82 | 26/19 | 294/4 | 153 | 1.055 | 0.222 | 035,70 |
| 114 | AG30 | Red bed | Triassic | 24 | 307/23 | 17/14 | 176/56 | 16/13 | 309/4 | 143 | 1.043 | 0.256 | 153,69 |
| 115 | TT1 | Red bed | Triassic | 12 | 087/11 | 66/18 | 299/77 | 22/12 | 267/3 | 132 | 1.023 | 0.505 | 250,75 |
| 116 | TT7 | Red bed | Triassic | 18 | 243/25 | 47/17 | 349/28 | 18/12 | 047/5 | 132 | 1.023 | 0.442 | 344,10 |
| 117 | AN1 | Red bed | Triassic | 11 | 132/14 | 39/17 | 277/73 | 17/10 | 312/8 | 133 | 1.021 | 0.357 | 310,68 |
| 118 | AN4 | Red bed | Triassic | 16 | 186/7 | 82/34 | 353/83 | 48/32 | 016/23 | 46.2 | 1.011 | 0.041 | 338,57 |
| 119 | AN5 | Red bed | Triassic | 17 | 275/42 | 31/14 | 098/47 | 27/14 | 098/5 | 118 | 1.011 | 0.246 | 104,42 |
| 120 | AN7 | Red bed | Triassic | 24 | 302/9 | 20/11 | 192/66 | 16/11 | 306/3 | 178 | 1.037 | 0.425 | 205,53 |
| 121 | AN8 | Red bed | Triassic | 5 | 103/5 | 29/5 | 214/75 | 21/8 | 102/8 | 143 | 1.04 | 0.592 | 181,79 |
| 122 | AN9 | Red bed | Triassic | 17 | 299/45 | 15/7 | 188/20 | 22/8 | 140/4 | 143 | 1.044 | 0.007 | 181,17 |
| 123 | AN12 | Red bed | Triassic | 13 | 136/32 | 16/8 | 032/21 | 24/10 | 146/3 | 119 | 1.024 | 0.056 | 020,45 |
| 124 | AN15 | Red bed | Triassic | 13 | 300/30 | 13/10 | 143/57 | 48/12 | 313/8 | 115 | 1.019 | -0.058 | 185,48 |
| 125 | AN16 | Red bed | Triassic | 14 | 131/13 | 26/11 | 292/76 | 11/6 | 311/1 | 93.7 | 1.069 | 0.494 | 304,76 |
| 126 | AN17 | Red bed | Triassic | 15 | 112/25 | 12/9 | 348/50 | 32/9 | 298/7 | 45.0 | 1.022 | 0.027 | 341,45 |

| | | | | | | | | | | | | | |
|---|---|---|---|---|---|---|---|---|---|---|---|---|---|
| 127 | AN18 | Red bed | Triassic | 12 | 177/38 | 43/8 | 302/36 | 24/12 | 352/2 | 446 | 1.119 | 0.617 | 333,47 |
| # | Site | Lithology | Age | n | D/I(Kmax) In situ | E11.1 ($e_{12}/e_{13}$) | D/I(Kmin) In situ | E11.3 ($e_{13}/e_{23}$) or $\alpha_{95}$ | D/I(Kmax) Corrected | Km ($10^{-6}$) | P’ | T | Bedding pole |

*Vertical axis rotation (VAR) from site data, + and – are clockwise and anticlockwise VARs, respectively (from Izquierdo-Llavall et al., 2018).

n = number of specimens

D/I (Kmax)=Declination and inclination of Kmax

D/I(Kmax) In sites with * corrected data shows values previous to vertical axis rotation

E11.1 ($e_{12}/e_{13}$), $e_{12}$ and $e_{13}$ are half confidence angles of Kmax from Jelinek’s statistics

E11.3 ($e_{13}/e_{23}$), $e_{13}$ and $e_{23}$ are half confidence angles of Kmin from Jelinek’s statistics

$\alpha_{95}$ = semiangle of the cone of confidence about the mean direction, from Fisher (1953)

Km = $(K_{max} + K_{int} + K_{min}) / 3$ (mean susceptibility, in $10^{-6}$ SI units)

P’ = $\exp\{2[(\eta_1 - \eta)^2 + (\eta_2 - \eta)^2 + (\eta_3 - \eta)^2]\}^{1/2}$ (corrected anisotropy degree; Jelinek, 1981)

T= $[2(\eta_2 - \eta_3) / (\eta_1 - \eta_3)] - 1$ [shape factor, -1 (prolate ellipsoid) to +1 (oblate ellipsoid); Jelinek, 1981]

o = overturned bedding

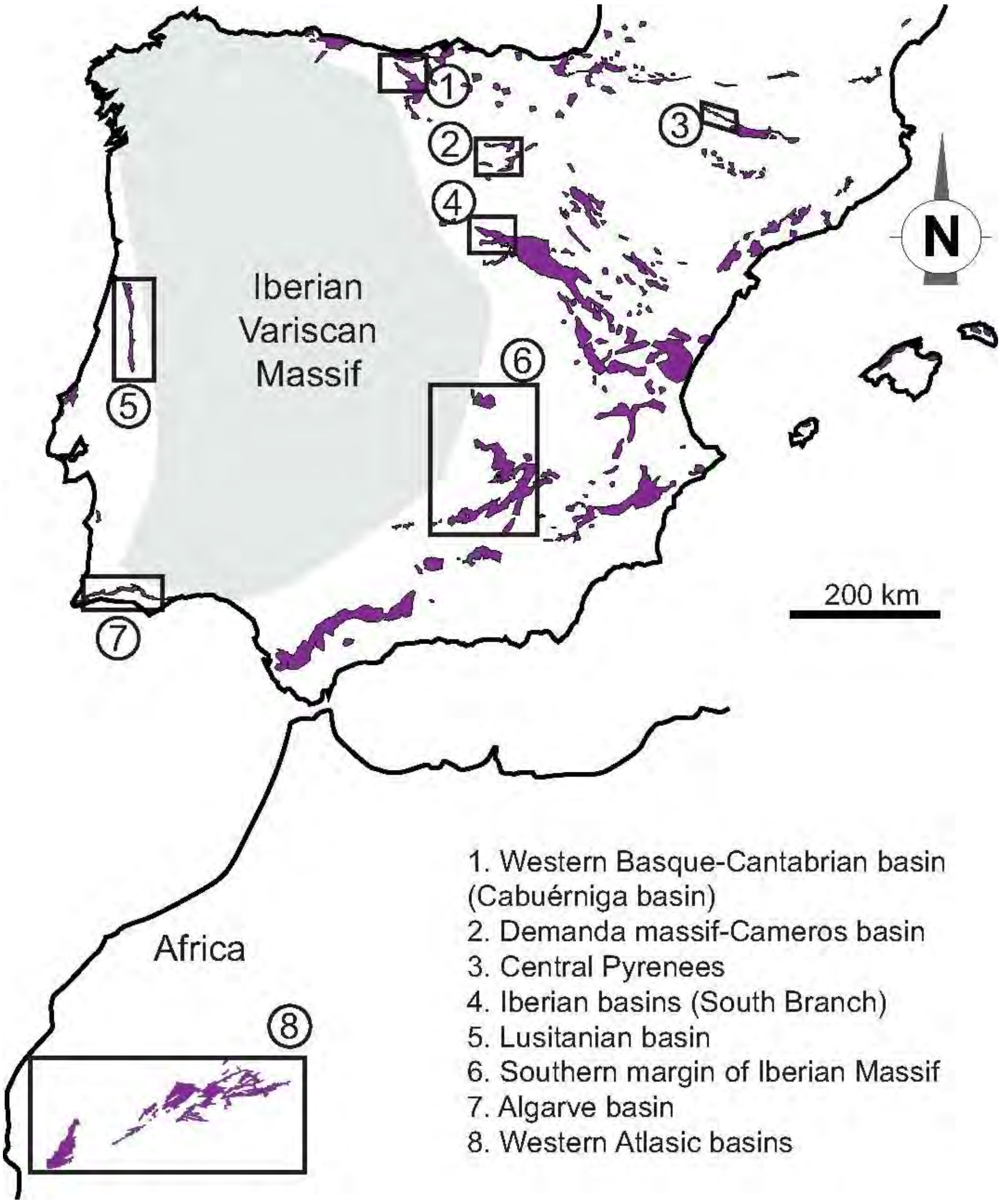
1
2
3
4
5
6
7
8
N
Iberian Variscan Massif
200 km
Africa
1. Western Basque-Cantabrian basin (Cabuérniga basin)
2. Demanda massif-Cameros basin
3. Central Pyrenees
4. Iberian basins (South Branch)
5. Lusitanian basin
6. Southern margin of Iberian Massif
7. Algarve basin
8. Western Atlasic basins

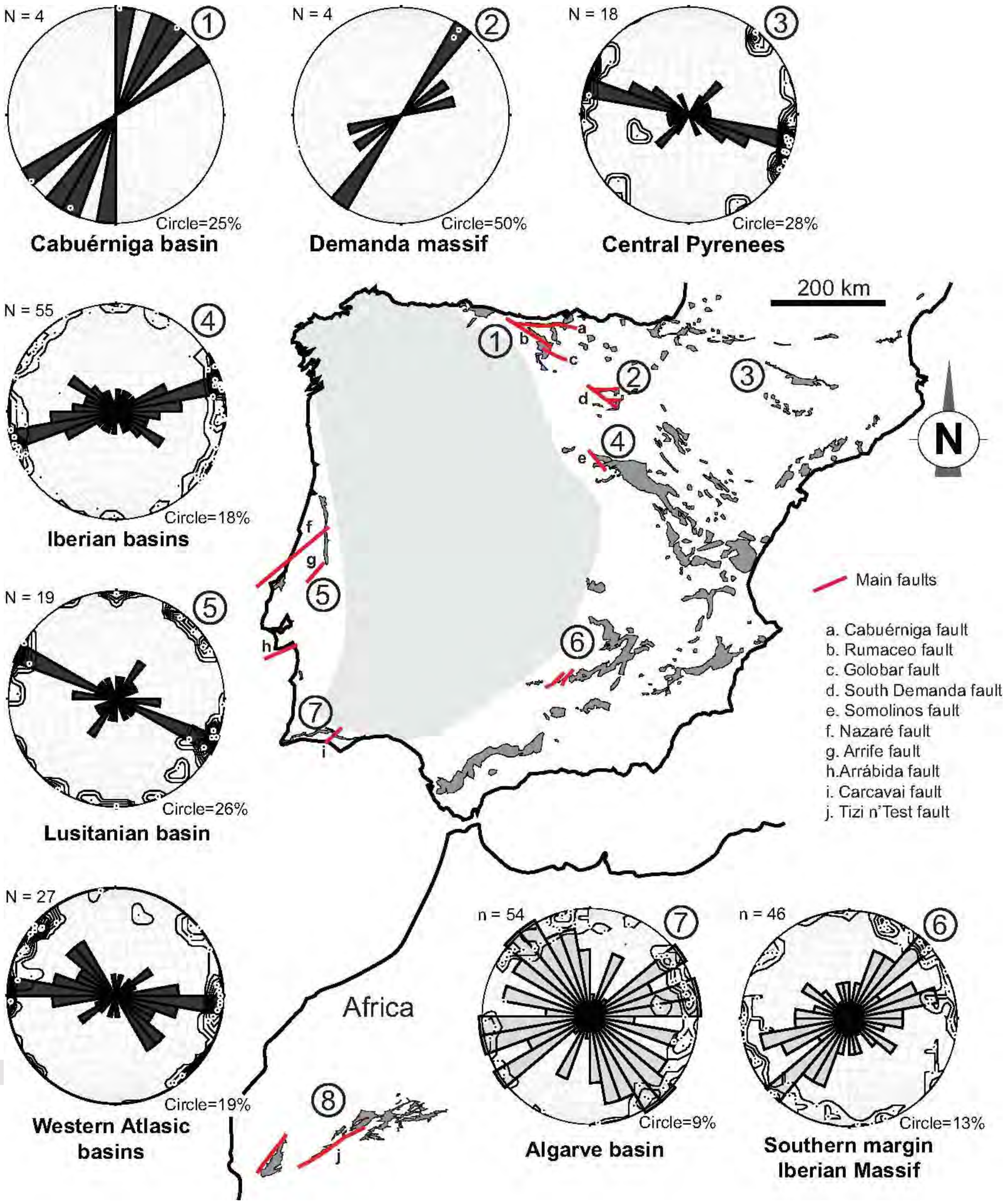
N = 4
①
Circle=25%
Cabuérniga basin
N = 4
②
Circle=50%
Demanda massif
N = 18
③
Circle=28%
Central Pyrenees
N = 55
④
Circle=18%
Iberian basins
N = 19
⑤
Circle=26%
Lusitanian basin
N = 27
Circle=19%
Western Atlasic basins
200 km
N
a
b
c
d
e
f
g
h
i
j
⑥
⑦
⑧
Africa
Main faults
a. Cabuérniga fault
b. Rumaceo fault
c. Golobar fault
d. South Demanda fault
e. Somolinos fault
f. Nazaré fault
g. Arrife fault
h.Arrábida fault
i. Carcavai fault
j. Tizi n'Test fault
n = 54
⑦
Circle=9%
Algarve basin
n = 46
⑥
Circle=13%
Southern margin Iberian Massif

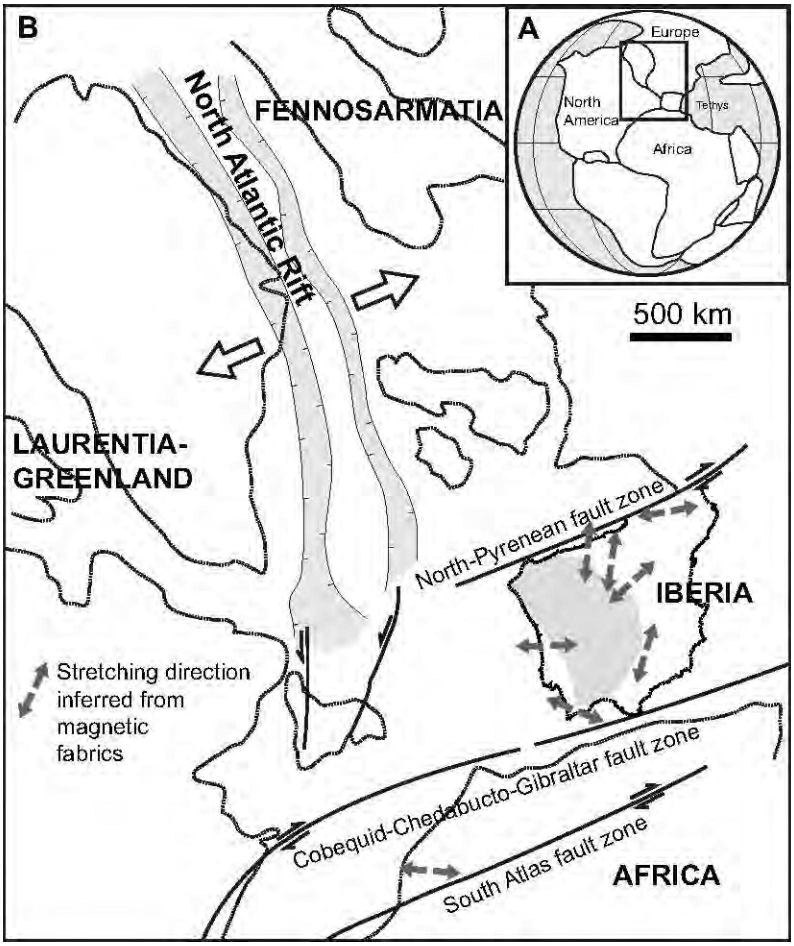
B
A
Europe
North America
Tethys
Africa
500 km
North Atlantic Rift
FENNOSARMATIA
LAURENTIA-GREENLAND
North-Pyrenean fault zone
IBERIA
Stretching direction inferred from magnetic fabrics
Cobequid-Chedabucto-Gibraltar fault zone
South Atlas fault zone
AFRICA

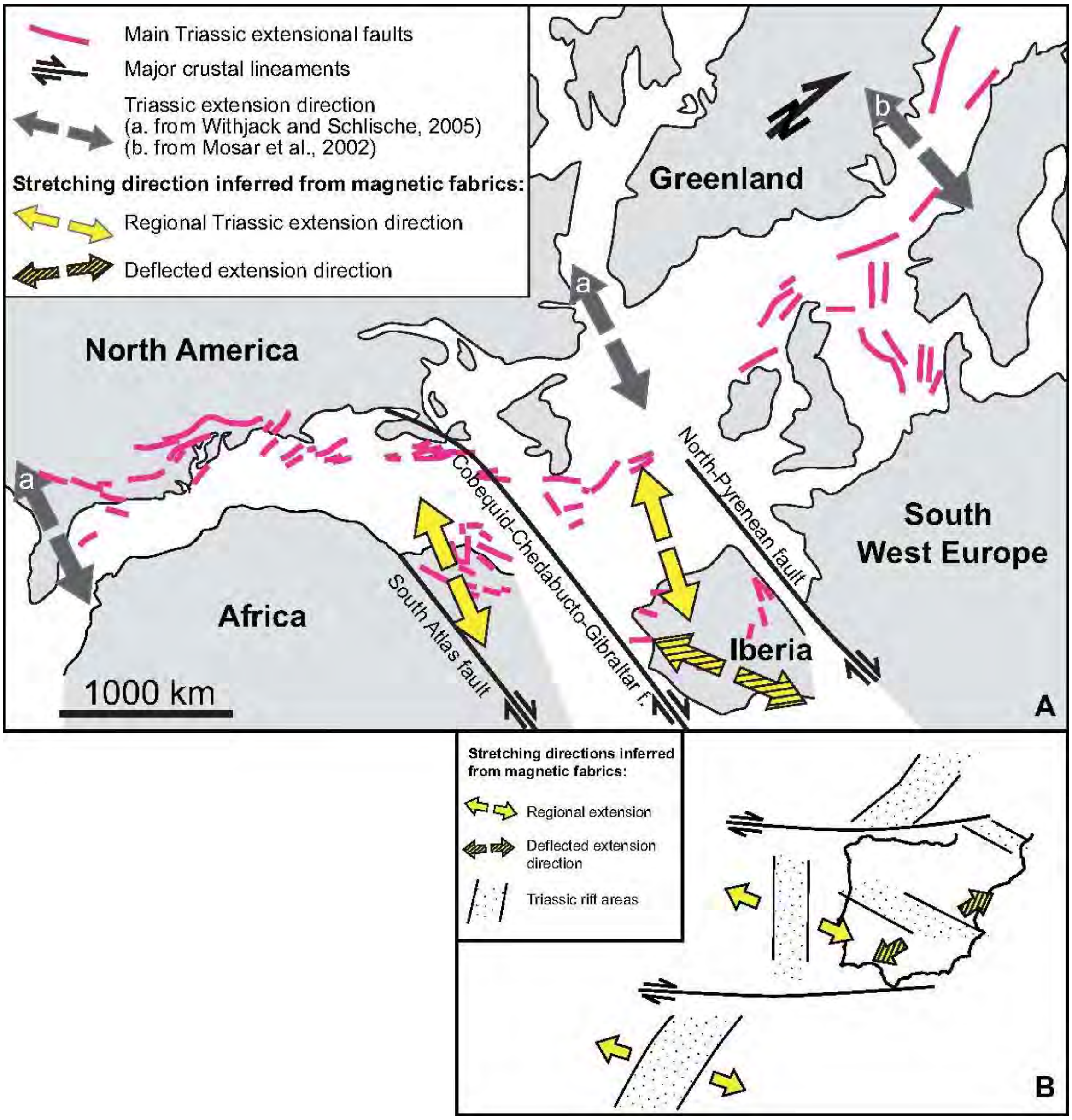
Main Triassic extensional faults
Major crustal lineaments
Triassic extension direction
(a. from Withjack and Schlische, 2005)
(b. from Mosar et al., 2002)
Stretching direction inferred from magnetic fabrics:
Regional Triassic extension direction
Deflected extension direction
North America
Greenland
South West Europe
Africa
Iberia
a
a
b
Cobequid-Chedabucto-Gibraltar f.
North-Pyrenean fault
South Atlas fault
1000 km
A
Stretching directions inferred from magnetic fabrics:
Regional extension
Deflected extension direction
Triassic rift areas
B